Supplement of Atmos. Chem. Phys., 17, 1673–1688, 2017
http://www.atmos-chem-phys.net/17/1673/2017/
doi:10.5194/acp-17-1673-2017-supplement

Atmospheric Chemistry and Physics Open Access EGU

Supplement of

Impact of biogenic very short-lived bromine on the Antarctic ozone hole during the 21st century

Rafael P. Fernandez et al.

Correspondence to: Alfonso Saiz-Lopez (a.saiz@csic.es)

1 Validation of CAM-Chem in the stratosphere

CAM-Chem, as well as WACCM, were part of CCMVal-2 and so were included in many of the papers comparing the evolution of stratospheric ozone (Eyring et al., 2010a) as well as the model sensitivity to different greenhouse scenarios (Eyring et al., 2010b). More recently, both CAM-Chem and WACCM participated in the CMIP5 inter-comparison project, computing stratospheric ozone interactively (Eyring et al., 2013a). Note that for those studies an identical geographical and altitude configuration as the one described here was used, and CAM-Chem return dates estimations is behaving very much in the middle of the simulated return periods of the multi-model range (see Fig.1 in Eyring et al., (2010a)).

Lamarque et al. (2008) showed that even when CAM has a relatively low model top (~40 km), the model shows good ability at reproducing a variety of large- scale changes in climate and chemical composition in the stratosphere when forced with the observed sea-surface temperatures and surface concentrations of long-lived trace gases and ozone-depleting substances. The model upward propagation of gravity waves (GW) due to the existence of a positive anomaly in the zonal wind distribution at mid-latitudes has the effect of increasing the momentum deposition associated with the GW, and indicates the presence of enhanced residual circulation (see Fig. 18 in Lamarque et al., (2008)). Additionally, (Lamarque and Solomon, 2010) analysed the role of long-term increases in CO_2, SST and halocarbons in explaining the observed trend of ozone in the tropical lower stratosphere using CAM-Chem (v3), and compared the model performance against WACCM (see their Fig. 1, vertical distributions of the tropical vertical velocity).

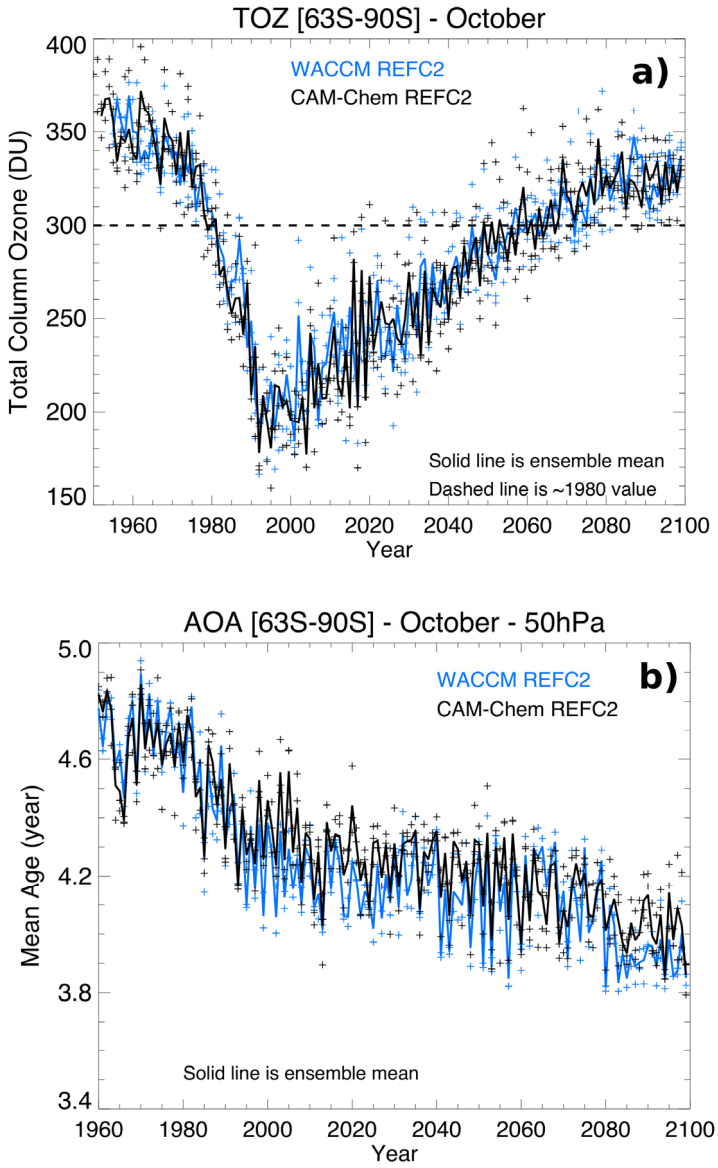

Figure S1: Comparison between CAM-Chem (black) and WACCM (light-blue) performance in the stratosphere for REFC2-CCMI simulations including the ~5 pptv additional VSL^{Br} contribution: A) Total ozone column averaged within the southern polar cap (TOZ^{SP}) during October; B). Mean Age of Air (AOA) at 50 hPa during October. CAM-Chem output correspond to the ensemble mean of three independent realizations (*sim*^{004}, *sim*^{005} and *sim*^{006}), while WACCM results correspond to a unique simulation. Note that the expected return date to 1980 Ozone levels is approximately the same for the two models.

CAM-Chem updates since WMO-2010 helped to improve the model performance. The implementation of a non-orographic gravity wave scheme for convection and fronts (originally developed for WACCM), as well as an inertia-gravity wave (IGW) parameterization, reduced stratospheric polar temperatures (which were biased warm) and increased chlorine activation and vortex size. As the limited vertical resolution (compared to

WACCM) does not allow the internal computation of the quasi-biennial oscillation (QBO), the QBO is imposed by relaxing equatorial zonal winds to the observed inter-annual variability. Additionally, stratospheric aerosol and surface area density data has been updated to the common observation-derived dataset for the CCMI project (Eyring et al., 2013b; Hegglin et al., 2014). A complete validation of current CAM-Chem version, focused on tropospheric issues but including total ozone column as well as stratospheric dynamics, is given in (Tilmes et al., 2016; see Figs. 2, 5 and 8).

References

Eyring, V., Arblaster, J. M., Cionni, I., Sedláček, J., Perlwitz, J., Young, P. J., Bekki, S., Bergmann, D., Cameron-Smith, P., Collins, W. J., Faluvegi, G., Gottschaldt, K. D., Horowitz, L. W., Kinnison, D. E., Lamarque, J. F., Marsh, D. R., Saint-Martin, D., Shindell, D. T., Sudo, K., Szopa, S. and Watanabe, S.: Long-term ozone changes and associated climate impacts in CMIP5 simulations, J. Geophys. Res. Atmos., 118, 5029–5060, doi:10.1002/jgrd.50316, 2013a.

Eyring, V., Cionni, I., Bodeker, G. E., Charlton-Perez, a. J., Kinnison, D. E., Scinocca, J. F., Waugh, D. W., Akiyoshi, H., Bekki, S., Chipperfield, M. P., Dameris, M., Dhomse, S., Frith, S. M., Garny, H., Gettelman, A., Kubin, A., Langematz, U., Mancini, E., Marchand, M., Nakamura, T., Oman, L. D., Pawson, S., Pitari, G., Plummer, D. a., Rozanov, E., Shepherd, T. G., Shibata, K., Tian, W., Braesicke, P., Hardiman, S. C., Lamarque, J. F., Morgenstern, O., Pyle, J. a., Smale, D. and Yamashita, Y.: Multi-model assessment of stratospheric ozone return dates and ozone recovery in CCMVal-2 models, Atmos. Chem. Phys., 10(19), 9451–9472, doi:10.5194/acp-10-9451-2010, 2010a.

Eyring, V., Cionni, I., Lamarque, J. F., Akiyoshi, H., Bodeker, G. E., Charlton-Perez, a. J., Frith, S. M., Gettelman, a., Kinnison, D. E., Nakamura, T., Oman, L. D., Pawson, S. and Yamashita, Y.: Sensitivity of 21st century stratospheric ozone to greenhouse gas scenarios, Geophys. Res. Lett., 37(16), n/a–n/a, doi:10.1029/2010GL044443, 2010b.

Eyring, V., Lamarque, J.-F., Hess, P., Arfeuille, F., Bowman, K., Chipperfield, M. P., Duncan, B., Fiore, A., Gettelman, A., Giorgetta, M. A., Granier, C., Hegglin, M., Kinnison, D., Kunze, M., Langematz, U., Luo, B., Martin, R., Matthes, K., Newman, P. A., Peter, T., Robock, A., Ryerson, T., Saiz-Lopez, A., Salawitch, R., Schultz, M., Shepherd, T. G., Shindell, D., Stähelin, J., Tegtmeier, S., Thomason, L., Tilmes, S., Vernier, J.-P., Waugh, D. W. and Young, P. J.: Overview of IGAC/SPARC Chemistry-Climate Model Initiative (CCMI) Community Simulations in Support of Upcoming Ozone and Climate Assessments, SPARC Newsl., 40(January), 48–66, 2013b.

Hegglin, M. I., Lamarque, J.-F., Eyring, V., Hess, P., Young, P. J., Fiore, A. M., Myhre, G., Nagashima, T., Ryerson, T., Shepherd, T. G. and Waugh, D. W.: IGAC/SPARC Chemistry-Climate Model Initiative (CCMI) 2014 Science Workshop, SPARC Newsl., 43(July), 32–35, 2014.

Lamarque, J. F. and Solomon, S.: Impact of changes in climate and halocarbons on recent lower stratosphere ozone and temperature trends, J. Clim., 23(10), 2599–2611, doi:10.1175/2010JCLI3179.1, 2010.

Lamarque, J.-F., Kinnison, D. E., Hess, P. G. and Vitt, F. M.: Simulated lower stratospheric trends between 1970 and 2005: Identifying the role of climate and composition changes, J. Geophys. Res., 113(D12), D12301, doi:10.1029/2007JD009277, 2008.

Tilmes, S., Lamarque, J., Emmons, L. K., Kinnison, D. E., Marsh, D., Garcia, R. R., Smith, A. K., Neely, R. R., Conley, A., Vitt, F., Martin, M. V., Tanimoto, H., Simpson, I., Blake, D. R. and Blake, N.: Representation of the Community Earth System Model (CESM1) CAM4-chem within the Chemistry-Climate Model Initiative (CCMI), Geosci. Model Dev., 9, 1853–1890, doi:10.5194/gmd-9-1853-2016, 2016.

2 Results for individual ensemble members

Figures S2-S3 show equivalent plots to Fig.2A and 2B in the main text, but considering each individual ensemble member instead of the ensemble mean. As all setups are independent one of the other, we present a 9-pannel figure where each of the run^{LL} realizations (004^{LL}, 005^{LL} and 006^{LL}) is compared against all of the run^{LL+VSL} simulations (004^{LL+VSL}, 005^{LL+VSL} and 006^{LL+VSL}), and viceversa. In all cases, the monthly-mean output for October, as well as a smoothed curve considering an 11-year hamming window is shown. Return dates values shown in Table 1 of the main text were extracted from these panels.

Figure S4 show equivalent plots to Fig. 5 in the main text, but includes the non-smoothed data. In this case, the daily output of the Total Ozone Colum was used to compute the Ozone Hole Area (OHA) and Ozone Mass Deficit (OMD) for each simulation, and the monthly mean for October was computed from the daily data. Only 3 of the 9 possible comparisons of independent ensemble members are shown.

The smoothed TOZ^{SP} and OHA timeseries present a large-scale oscillation that appears randomly for each independent simulation, which introduces local maxima and/or minima at different periods of time. Even when the oscillations are reduced when the ensemble mean is computed, they still appear when the differences between sim^{LL+VSL} and sim^{LL} are computed (as well as when any couple of independent simulations are considered). We've performed different types of smoothing (moving average, hamming filter, etc.) and/or variable window widths (between 5 and 20 years) to perform the fit, and found no dependence on the filter nor the smoothing window used. We've assigned these random oscillations to the intrinsic free-running model variability between the individual ensemble members, and suggested increasing the number of realizations and/or using other chemistry-climate models in order to reduce the uncertainties.

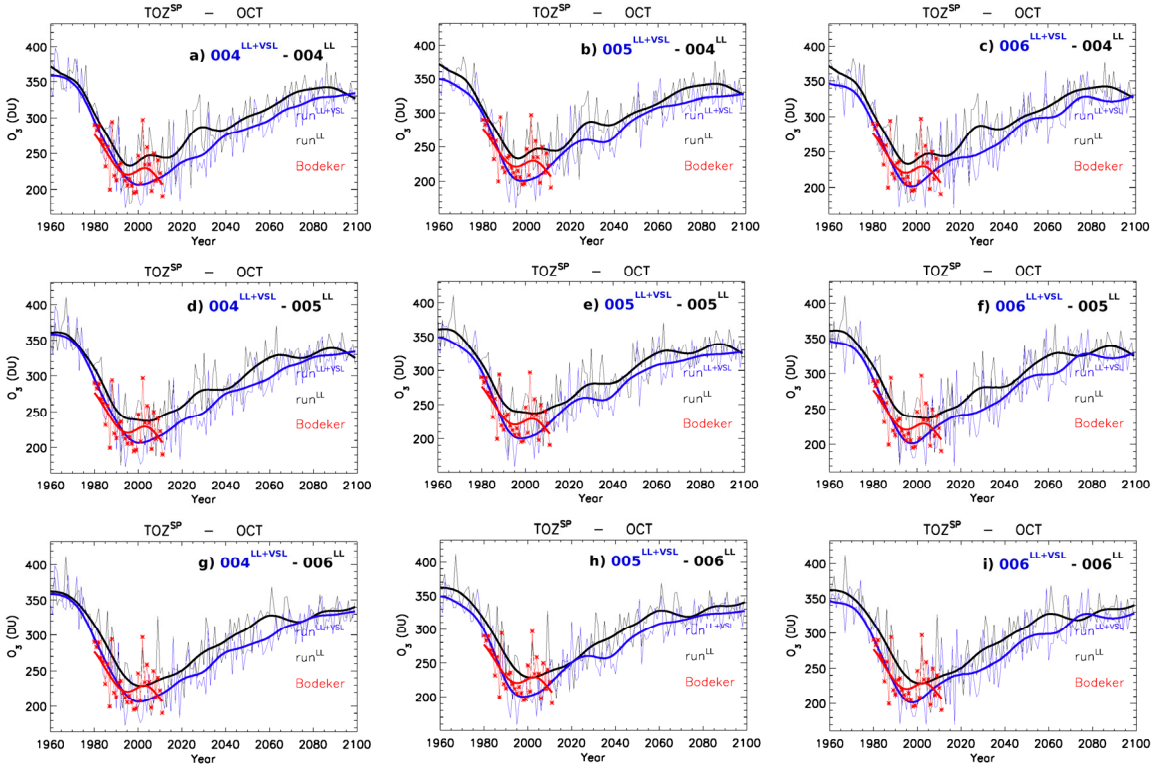

Figure S2: Temporal evolution of the absolute total ozone column averaged within the southern polar cap (TOZ^{SP}) during October. The monthly TOZ^{SP} mean for each independent ensemble (thin lines) as well as the 11-years smooth timeseries (thick lines) is shown in blue for run^{LL+VSL} and black for run^{LL}. Red lines and symbols show merged satellite and ground base measurements from the Bodeker database averaged within the same spatial and temporal mask as the model output. Equivalent results for the model ensemble mean are shown in Fig. 2A of the main text.

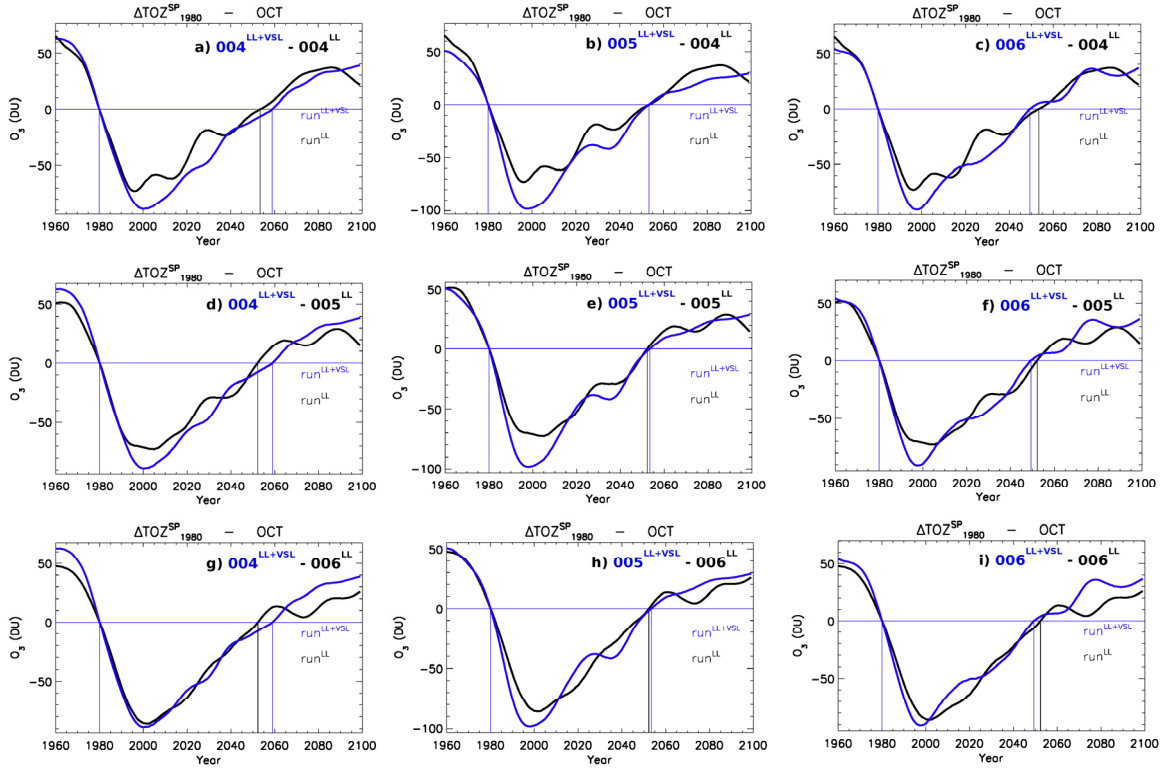

Figure S3: Temporal evolution of the total ozone column relative to October 1980 ($\Delta TOZ^{SP}_{1980} = TOZ^{SP}_{year} - TOZ^{SP}_{1980}$). The zero horizontal line indicates the October ΔTOZ^{SP}_{1980} column for each experiment, while their respective return dates to 1980 are shown by the vertical lines. Equivalent results for the model ensemble mean are shown in Fig. 2B in the main text.

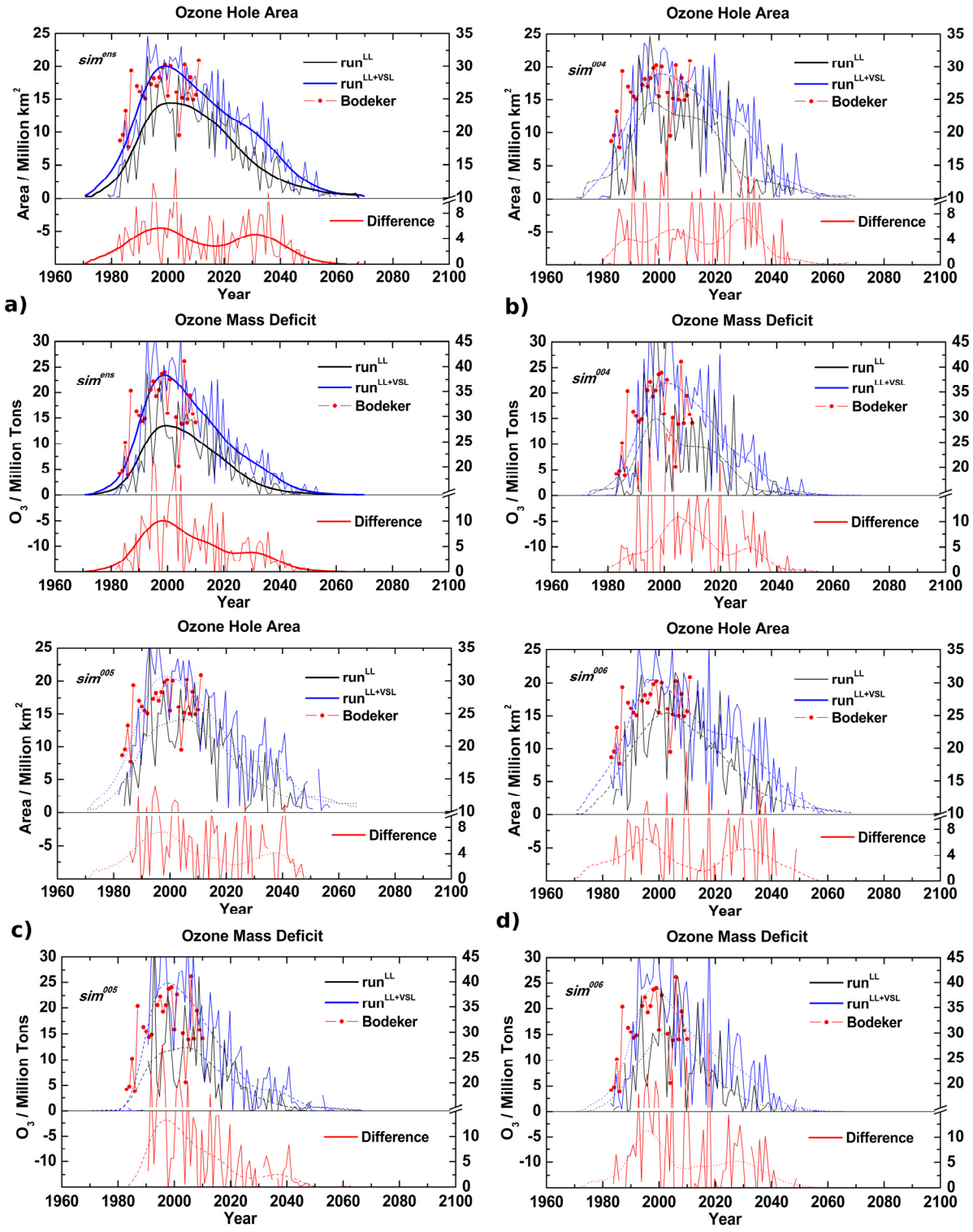

Figure S4: Temporal evolution of the ozone hole area (top) and ozone mass deficit (bottom) for *run*^{LL} (black) and *run*$^{LL+VSL}$ (blue) simulations (left axis), as well as the difference between runs (red, right axis). Thin lines show the October monthly mean value for each independent simulation, while the thick/dotted/dashed lines show the smoothed curve considering an 11-year Hamming window for a) *sim*^{ens}; b) *sim*^{004}; c) *sim*^{005}; and d) *sim*^{006}.